INTERNATIONAL JOURNAL OF AUTOMOTIVE AND MECHANICAL ENGINEERING
ISSN: 2229-8649 e-ISSN: 2180-1606
VOLUME 22, ISSUE 4, 2025, 12986 - 13001
DOI: https://doi.org/10.15282/ijame.22.4.2025.11.0988

RESEARCH ARTICLE

Flow Structure Control Over the Square Cylinder with Inclined Splitter Plate: A Pathway to Conserving Energy

La Ode Ahmad Barata[1]*, Takahiro Kiwata[2], Sudarsono[1], Sayahdin Alfat[3], Nanang Endriatno[1], Rudi Purwo Wijayanto[4]

[1]Mechanical Engineering Department, Universitas Halu Oleo, 93232, Kendari, Indonesia
[2]Institute of Science and Engineering, Kanazawa University, Japan
[3]Physic Education Science, Halu Oleo University, Indonesia
[4]National Research and Innovation Agency, Indonesia

ABSTRACT – Flow control over a square cylinder using an attached double splitter plate was numerically investigated at a Reynolds number of 10^4. This study aimed to investigate the effects of the splitter plate and angle of incidence on fluid forces, pressure distributions, and vortex-shedding. The two plates were positioned ¾ H apart, with various inclination angles. The vortex shedding frequency was typically obtained from lift fluctuation measurements, while the aerodynamic force coefficients acting on the model were determined from pressure distributions. This investigation explored characteristics of the vortex formation region, the location of flow separation, and reattachment points. The process also included the gradient pressure recovery corresponding to a minimum drag coefficient reduction. Suppressing lift fluctuation by tilting the plate $\alpha \geq 10°$ negated drag reduction. It was attributed to the pressure gradient effect rather than solely to lift fluctuation frequency. At zero angle of incidence (α), the drag coefficient of a square cylinder decreased by approximately 39.3%. Drag reduction was maximum at about $\alpha \leq 5°$ and reached the peak reduction at $\alpha = 2.5°$, with a 43.8% reduction compared to the bare square cylinder. Additionally, drag reduction achieved with the double splitter plate was twice that of the single splitter, achieving about 20.3%. This study recommended an optimal drag reduction by tilting the plate at an angle of 5 ° or less. Drag reduction provides a means to reduce the energy required to move objects.

ARTICLE HISTORY
Received : 30th Jul. 2024
Revised : 03rd Jul. 2025
Accepted : 01st Aug. 2025
Published : 11th Nov. 2025

KEYWORDS
Turbulence control
Drag reduction
Flow-structure interaction
Bluff body
Flow field

1. INTRODUCTION

Flow-structure interaction is becoming a fundamental subject in fluid dynamics, due to its critical role in the performance, stability, and energy efficiency of various engineering systems. Unsteady flow phenomena often occur in practical applications such as vehicles, missiles, heat exchangers, masts, long piping systems, cable grids, marine risers, chimneys, cooling towers, and tall skyscrapers, where the appliances can generate significant aerodynamic drag as well as flow-induced vibrations. Subsequently, the behavior of fluid flow around a structural cylinder has been reported in both experimental and numerical literature [1] – [3]. The interaction between a structure and the surrounding flow can give rise to flow-induced vibrations and aerodynamic problems, including structural failure (as exemplified by the collapse of the Tacoma Narrows Bridge [4]), environmental noise in cable lines [5], and increased fuel consumption in vehicles [6].

Vortex shedding occurs when fluid flows through an object, producing alternating vortices in its wake that can generate unwanted noise, vibrations, and unstable aerodynamic forces. To mitigate these effects, a splitter plate is often introduced to manipulate the flow and suppress the negative impact on various engineering structures, including marine pipelines, bridge structures, automotive components, marine moving objects, tall buildings, and other constructions exposed to strong wind or water currents [6] – [8]. The shape of cylinder objects plays a crucial role in determining fluid flow behavior, making it essential to conduct extensive investigations to identify an effective method for analyzing flow patterns and achieving efficient aerodynamic design. Studies have shown that reducing vortex interactions can effectively suppress adverse effects, including excessive vibrations, increased dynamic loads, and accelerated structural damage [9]–[11]. Several methods for preventing the impact of vortex shedding or its direct interaction with a circular cylinder have been described by [12]. Moreover, this study discussed the use of various flow-control methods for a circular cylinder, including surface protrusion, a shroud, a perforated plate, guiding vanes, and a splitter plate. A splitter plate is a crucial flow-control device in many engineering applications, mitigating the negative effects of flow dynamics and enhancing heat transfer efficiency. This impact helps improve designs to enhance the effectiveness, stability, and control of fluid dynamics or heat transfer. Additionally, fluid flows tend to generate vortices, which are whirling pockets of fluid located on the sides and behind the cylinder. By addressing this issue, the splitter plate can create a more consistent and predictable flow pattern.

Another method for controlling flow behavior was conducted using a parallel splitter plate downstream. Studies have shown that the use of a double splitter plate can effectively control fluctuating lift and drag forces, reduce the frequency

*CORRESPONDING AUTHOR | L. O. A. Barata | ✉ ahmad.barata@uho.ac.id

of vortex shedding, and increase base pressure more effectively than using a single plate [13]. Further investigation revealed that the dual splitter plate configuration is optimal for enhancing drag reduction and mitigating lift fluctuations. A study conducted by [14] also investigated the interaction between the upstream splitter plate. The result showed that the upstream plate reduced the effective length of the downstream plate and increased vortex shedding downstream. Vortex shedding imposes a dynamic load on the cylinder, thereby increasing the risk of structural failure. This problem could be prevented by installing plates on both upstream and downstream sides of the object. When handling an elastically mounted cylinder, the splitter plate affected the damping system. In this study, an alternative method was employed to benefit from the plate, utilizing a detached, flexible, or slotted splitter plate [15], [16].

When using a splitter plate as a passive device to control turbulence around both rectangular and circular cylinders, it is necessary to consider the critical gap, the design of the detached splitter plate, and the variation in plate length. The difference in separation points between cylinder types is essential when adjusting the gap and length of the plate. Furthermore, the reattachment of the separated shear layer downstream of the detached splitter plate influences the flow features around the structure [17], [18]. Further investigation of the reattachment effect of the shear layer on the dynamic response of an elastically mounted slender object has been conducted [19]. The result showed that the detached splitter effectively stabilized the transverse dynamic response of the rectangular prism and reduced the incidence of galloping. These features were significant for developing an energy harvester from fluid-induced vibrations (FIV) [20], [21]. However, the effectiveness of using a splitter plate as a flow control device depends on factors, including its shape, dimensions, number, and position. The efficiency is also influenced by specific engineering objectives, in aerodynamics applications or heat transfer [22], [23].

The flow around the cylinder was divided symmetrically by a straight splitter plate. The parallel downstream plate prevented unsteady, symmetrical vortices from growing and interacting in the wake, resulting in a stable flow pattern. Additionally, lift force is an aerodynamic force component that is perpendicular to the flow direction. The angle of inclination of the plate affected the direction of lift due to unequal diversion of flow. In the case of vortex shedding control, an inclined splitter plate might be more efficient than straight ones [17], [18].

Passive flow control is employed in a splitter plate to reduce the total drag force, simplify the flow, and manage vortex shedding downstream. This was an essential method when reducing resistance force was crucial, such as with wind truck deflectors and airplane wings. Alternatively, the splitter plate had a complicated effect on the heat transfer process. An angled splitter plate on a square cylinder offered an interesting twist to the flow behavior. In some circumstances, heat transfer from the object could be reduced by stabilizing the flow of the plate. Moreover, a study by [24] installed an inclined double splitter plate on the square's side surface to improve heat dissipation. The plate-modified flow structure in the wake also improved heat transfer by up to 40.7%. This study showed time-averaged drag reduction and root mean square (RMS) lift increment. In another case, an inclined plate was also arranged in a circular cylinder downstream by [17], who observed the effect of an angled splitter on the suppression of vortex-induced vibrations (VIV). Regarding this discussion, the investigation revealed that tilting the plate by more than 5° created a significant pressure gradient, and the generation of secondary vortices downstream was attributed to the suppression of crossflow vibration.

Previous studies [24]–[26] focused on a single or double splitter plate, either numerically or experimentally, whereas this study focuses on using a double downstream plate with various inclined angles. Gap [12], [18] and length of splitter plate [13]. [25] have a significant effect on flow quantities, dynamic response, and heat dissipation. However, the effect of the varying angle of the splitter plate behind the cylinder has not been extensively examined. Therefore, this study aims to examine flow characteristics around a square shape with a double splitter plate positioned downstream. Considering this perspective, the angle of the splitter plate was changed to acquire a new understanding of flow pattern behaviors around a square cross-section. This optimization can provide valuable recommendations for drag reduction in this field.

2. NUMERICAL APPROACH

This study used an unsteady Reynolds-Averaged Navier-Stokes (*u*RANS) model because of the ability to effectively simulate time-dependent turbulent flows while maintaining a balance between computational cost and accuracy. The model provided a suitable balance between the computationally intensive Large Eddy Simulation (LES) and Direct Numerical Simulation (DNS). Therefore, the model was commonly used in engineering applications that required an understanding of unstable effects. This example was adapted to a variety of flows, making it a useful tool for solving engineering problems [27], [28]. Although LES and DNS provided more comprehensive flow data, the methods were often too expensive for many engineering practices. Meanwhile, uRANS offered a middle ground, providing good accuracy at a more acceptable computational cost [29].

2.1 Governing Equations

This study focused on a two-dimensional analysis of unsteady flow characteristics as fluid passed around a square cylinder with an attached downstream splitter plate. The solution was based on an unsteady RANS model with the Realizable $k - \varepsilon$ turbulence model. In addition, this model examined incompressible Newtonian flow, incorporating equations for mass and momentum conservation below.

- Two-dimensional continuity equation for incompressible flow:

$$\frac{\partial u_i}{\partial x_i} = 0, \tag{1}$$

indices i = 1 and 2 (for 2D case), representing streamwise and crossflow direction, respectively.

- Navier–Stokes Momentum Equation of Newtonian fluid flow in 2D Cartesian coordinates

$$\rho g_x - \frac{\partial P}{\partial x} + \mu\left(\frac{\partial^2 u}{\partial x^2} + \frac{\partial^2 u}{\partial y^2} + \frac{\partial^2 u}{\partial z^2}\right) = \rho\left(\frac{\partial u}{\partial t} + u\frac{\partial u}{\partial x} + v\frac{\partial u}{\partial y}\right) \tag{2}$$

$$\rho g_y - \frac{\partial P}{\partial y} + \mu\left(\frac{\partial^2 v}{\partial x} + \frac{\partial^2 v}{\partial y^2} + \frac{\partial^2 v}{\partial z^2}\right) = \rho\left(\frac{\partial v}{\partial t} + u\frac{\partial v}{\partial x} + v\frac{\partial v}{\partial y}\right) \tag{2a}$$

- Realizable $k - \varepsilon$ (RKE) turbulence model

The resolved kinetic energy (RKE) model was a two-equation eddy viscosity model used in computational fluid dynamics (CFD) to simulate average flow characteristics of turbulent flows. The turbulence model was used to solve two transport equations, such as the turbulent kinetic energy (TKE) equation and the turbulent dissipation rate (ε). TKE described the transport of turbulent kinetic energy, which measured the intensity of turbulence. Meanwhile, ε represented transport of turbulent dissipation rate, indicating how quickly turbulent kinetic energy was converted into heat. These equations could be used to solve turbulent viscosity (μ_t) as expressed in Equations 3 and 4, and model Reynolds stresses in the Navier-Stokes equations. RKE provided improved accuracy compared to standard $k - \varepsilon$ for a wide range of CFD simulations, including flows with rotation, boundary layers under strong adverse pressure gradients, separation, and recirculation. However, the method was less accurate than some other turbulence models for certain types of flows, such as highly swirling flows [29].

$$\frac{\partial}{\partial t}(\rho K) + \frac{\partial}{\partial x_i}(\rho K u_i) = \frac{\partial}{\partial x_j}\partial\left[\left(\mu + \frac{\mu_t}{\sigma_k}\right)\frac{\partial k}{\partial x_j}\right] + G_k + G_b - \rho\varepsilon - Y_M + S_K \tag{3}$$

$$\frac{\partial(\rho\varepsilon)}{\partial t} + \frac{\partial(\rho\varepsilon u_i)}{\partial x_i} = \frac{\partial}{\partial x_j}\left[\left(\mu + \frac{\mu_t}{\sigma_\varepsilon}\right)\frac{\partial \varepsilon}{\partial x_j}\right] + \rho C_1 S_{\varepsilon -}\rho C_2 \frac{\varepsilon^2}{K + \sqrt{v\varepsilon}} + C_{1\varepsilon}\frac{\varepsilon}{K}C_{3\varepsilon}G_b + S_\varepsilon \tag{4}$$

where:

$$C_1 = \max.\left[0{,}43, \frac{\eta}{\eta+5}\right],\ \eta = s\frac{k}{\epsilon},\ \mathrm{s} = \sqrt{2s_{ij}s_{ij}} \tag{4a}$$

G_b and G_k represented turbulent kinetic generation due to time-average gradient velocity and buoyancy effect, respectively. Y_M represented fluctuating dilatation because of the compressibility effect, and C_i were constants. In addition, the term of σ_k and σ_ε was a turbulent Prandtl Number for k, as well as ε, and S_i were source terms. The set of RANS equations was solved by using a finite volume solver called ANSYS Fluent. For discretization, the second-order upwind method was applied to the governing equations, as well as to the TKE and dissipation rate equations. Also, the second-order implicit transient formulation and the pressure-velocity coupling SIMPLEC algorithm were used for time integration and momentum balance.

2.2 Computational Model

The schematic model of the computational domain of a square cylinder with a double splitter plate is shown in Figure 1. The square cylinder had a cross-section height (H) of 40 mm with an attached splitter plate of 3H. Furthermore, a two-dimensional grid domain was developed with upstream and downstream distances of 15H and 30H from the cylinder centerline, respectively. This leads to a blockage ratio of 5%, which was quite identical to the works verified by reference [30]. Following this discussion, the total number of grid points was 10^5 nodes with a minimum grid height of 5×10^{-3}. The first layer height (minimum grid) perpendicular to the wall boundary condition was determined by considering wall stress (τ_w), defined by Equation 5.

$$y^+ = \frac{y}{\mu}\sqrt{\rho\tau_w} \tag{5}$$

Non-dimensional layer height (y^+) and inflation of the grid layer near the wall were determined according to the reference [31]. This study set the initial y^+ to 1, which was lower than the acceptable value prescribed by references [32], [33] for the RANS turbulence model, to ensure better near-wall resolution. Based on those previous references, the mesh resolution was adjusted to be more refined around the cylinder and splitter plate, where high flow separation was expected to occur. Since the simulation model was a fully implicit method, the time step size (Δt) was determined by considering computational time. Following the process, the Courant stability criterion ($C=1=u\Delta t/\Delta x$ was considered an initial reference, where u and Δx represented the velocity component as well as the first cell height of the adjacent wall [32]. Reynolds number, Re (= $\rho U_\infty/\mu$) of 10^4, where ρ and μ were density and dynamic viscosity of the fluid, respectively, and U_∞ represented uniform free-stream velocity. A non-slip condition specified as $u = 0$ was applied to the cylinder and wall surface boundary conditions. Moreover, symmetry planes, in which a frictionless wall was adopted at the bottom as well as the top of the domain, and an outflow boundary condition was applied at the far downstream outlet.

2.3 Model Verification and Validation

Non-dimensional layer height (y^+) mentioned in the previous section was prescribed in meshing construction by considering eddy motion in the viscous sublayer (y^+<5). Moreover, the process was conducted because the model had potential for high flow separation. The result showed that the y^+ maximum calculation was 9.62 for a square cylinder, which meant it was under the transition region. The value was in the recommended limit of 11.067, according to reference [29]. The calculation considered that the viscous stress was linear to the wall distance according to references [29], [30]. However, the mean calculated of y^+ for the angled splitter plate was 0.7 – 0.9, and it was less than the prescribed value in the initial mesh construction. The process showed a good agreement with the initial y^+ calculation as reviewed in references [34], [35]. The residual parameters, namely continuity, velocity, as well as energy components, were set to 10^{-6} and monitored for the convergence criterion as described in references [34], [35]. Additionally, the flow features past a square cylinder were analyzed and then extended to the model with a double attached splitter plate.

Table 1 showed that the drag coefficient (*CD*) of the 2D model was slightly lower than that of the 3D model and experimental data, while the Strouhal frequency data was less sensitive to the Reynolds numbers (*Re*) investigated. The existing data for the *CD* parameter were approximately 2.0 (moderate Re; 10^4 < Re < 10^5), signifying reasonable agreement with this study. In addition, the variation in *CD* was significantly affected by the three-dimensionality of the wake structure, turbulence model, and boundary layer transitions [36], [37]. Table 2 shows the effect of the splitter plate on global quantities (*CD*, *St*). The outcomes signified that preventing vortex shedding interaction in the cylinder downstream reduced the *CD* parameter. These features were agreed with experiment data [38], [39], for both single and double splitter plates. The *CD* value reduced at the flow regime near high *Re* [37], which was distinctly different from moderate *Re*. Moreover, variation of the *CD* values was considered due to different setting parameters of the splitter plate, such as length and arrangement of the splitter plates, and the numerical model. Table 3 showed that the global quantity (*CL*) fluctuation was also verified against local quantity (*u*) fluctuation, where parameters signified an acceptable deviation with an error less than 1%.

Table 1. Global quantities comparison of the flow past the plain square cylinder

	CD	-CPb	St	Re	Remark
Mizukami [38]	2.15	1.43	0.12	2.2×10^4	LES 3D
Yu [39]	2.14	1.56	0.14	1.0×10^4	LES 3D
Sohankar [40]	2.20	1.57	0.12	1.0×10^4	LES 3D
Lyn [41]	2.16	1.43	0.13	1.3×10^4	Exp.
Knisley [42]	2.03		0.13	2.2×10^4	Exp.
Shimada and Ishira [43]	2.05		0.14	2.2×10^4	RKE 2D
Present	2.01	1.30	0.12	1.0×10^4	RKE 2D

Table 2. Effect of the straight splitter plate on the global quantities

	CD	St	Re	Turbulence control	Remark
Present	1.60	0.075	1.0×10^4	Single SP	RKE 2D
Sharma and Dutta [44]	1.67	0.053	2×10^3	Single SP	Experiment
Ogunremi [45]	1.21– 1.38	n/a -	7.4×10^4	Single SP	Experiment
Dash et al. [13]	1.19	0.121	10^2	Double SP	LBM 2D
Wang [46]	1.25	0.059	1×10^4	Double SP	Exp.
Present	1.22	0.14	1×10^4	Double SP	RKE 2D

Table 3. Standard error for Strouhal frequency

Alfa (deg.)	$St_{,u'}$	$St_{,CL'}$	St_{Error} $(N_1-N_2/N_1)\times100\%$
0	0.1404	0.1402	0.140%
2.5	0.1424	0.1424	0%
5.0	0.1424	0.1435	-0.080%
7.5	0.1424	0.1424	-0.002%
10.0	0.1343	0.1343	0.000%
12.5	0.1227	0.1227	0%
15.0	0.1114	0.1117	-0.029%
17.5	0.1014	0.1008	0.630%
20.0	0.0920	0.0920	0.020%

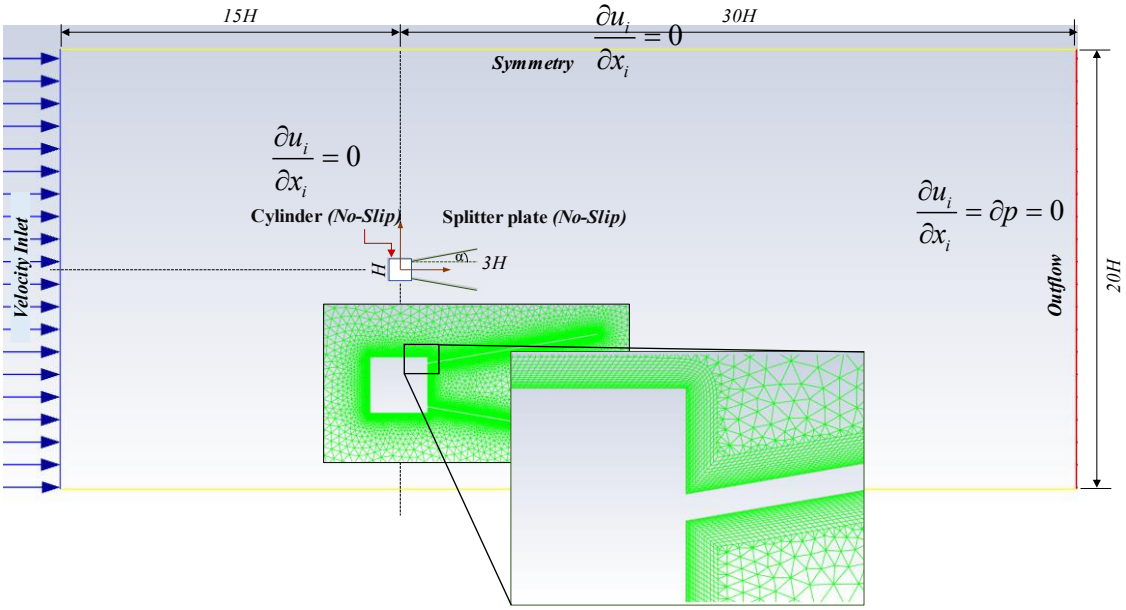

Figure 1. Computational domain

3. RESULTS AND DISCUSSION

3.1 Effect of angled splitter plate on aerodynamic forces

By preventing the interaction of the separated shear layer at the trailing edge, the aerodynamic forces of flow passing through the cylinder were significantly suppressed. This process was achieved by inserting a turbulence control device at the cylinder base. Parallel plates situated in the direction of flow improved drag reduction compared to a single plate, as shown in Table 2. Meanwhile, the effect of inclination angle variation of the parallel plate on the global quantities of flow passing through the square cylinder was shown in Figure 2(a). The effect of flow redirection potentially reduced vortex shedding fluctuation by inclining the splitter plate, and offered drag reduction compared to a straight splitter plate (α = 0°) on a square cylinder. Increasing splitter angle $\alpha > 10°$ negated drag reduction, while preserving time-average lift force uptick up to $\alpha = 10°$. Following this discussion, Figure 2(b) shows drag component reduction compared to a plain cylinder. The drag component suppressed up to 44% compared to the plain cylinder, and nullified it at $\alpha > 10°$. The drag reduction behavior was connected to the base pressure characteristic, as shown in Figure 2(c).

Figure 2 (c) shows the effect of inclining the splitter plate on base pressure. This quantity was closely related to the flow drag reduction behavior acting on the cylinder. During the process, the splitter plate maintained pressure recovery for plate angles less than 5°, but the recovery continuously reduced with increasing inclination angle. At higher inclinations ($\alpha > 10°$), the pressure recovery was insufficient to maintain lower drag due to flow separation at the trailing edge of the splitter plate, which induced more negative pressure than at the base of the cylinder, as shown in Section 3.3. Therefore, the downforce mechanism differed significantly from that of a plain cylinder, as the negative base pressure induced by the plate dominated the drag variation.

Figure 3 (a) shows the effect of the splitter plate on lift component profiles. When inserting a plate as a passive turbulent control to suppress lift fluctuation, a significant change in lift suppression was observed at $\alpha < 10°$. Lift suppression (downforce) potentially reduced the dynamic load of the structure by reducing the alternating vortex shedding in the wake. Additionally, a suppression lift component with a downstream splitter plate altered the vibration mechanism by creating lift instability, which depended on system damping and plate length [47]. Previous studies [6], [48] revealed that aerodynamics/hydrodynamics downforce improves the mileage of vehicles, watercraft, and weapons etc.

For the Strouhal numbers component, vortex shedding frequency was approximated by considering the lift component fluctuation and verified by measuring the velocity component (u) fluctuation downstream as recommended by [49]. The standard error was a maximum of 0.6% for an angled splitter plate of 15°, as shown in Table 3. Moreover, another study, such as [19], measured vortex shedding frequency by considering local velocity fluctuation at a specific point in the downstream position with X and Y coordinates of $4H$ and $1.5H$. This exploration showed that both lift and local velocity fluctuation frequency were reasonably matched. In addition, the end effect of the splitter plate changed the flow pattern downstream and interfered with the measurement point of local velocity, u (shedding pattern). The study proposed that the plate inclination was a maximum of 5° to achieve optimum drag reduction while maintaining base pressure recovery. Meanwhile, the St parameter showed a reasonable steadiness at $0° < \alpha < 5°$. Previous explorations showed that CD and CPb components were in an interdependent relation [39].

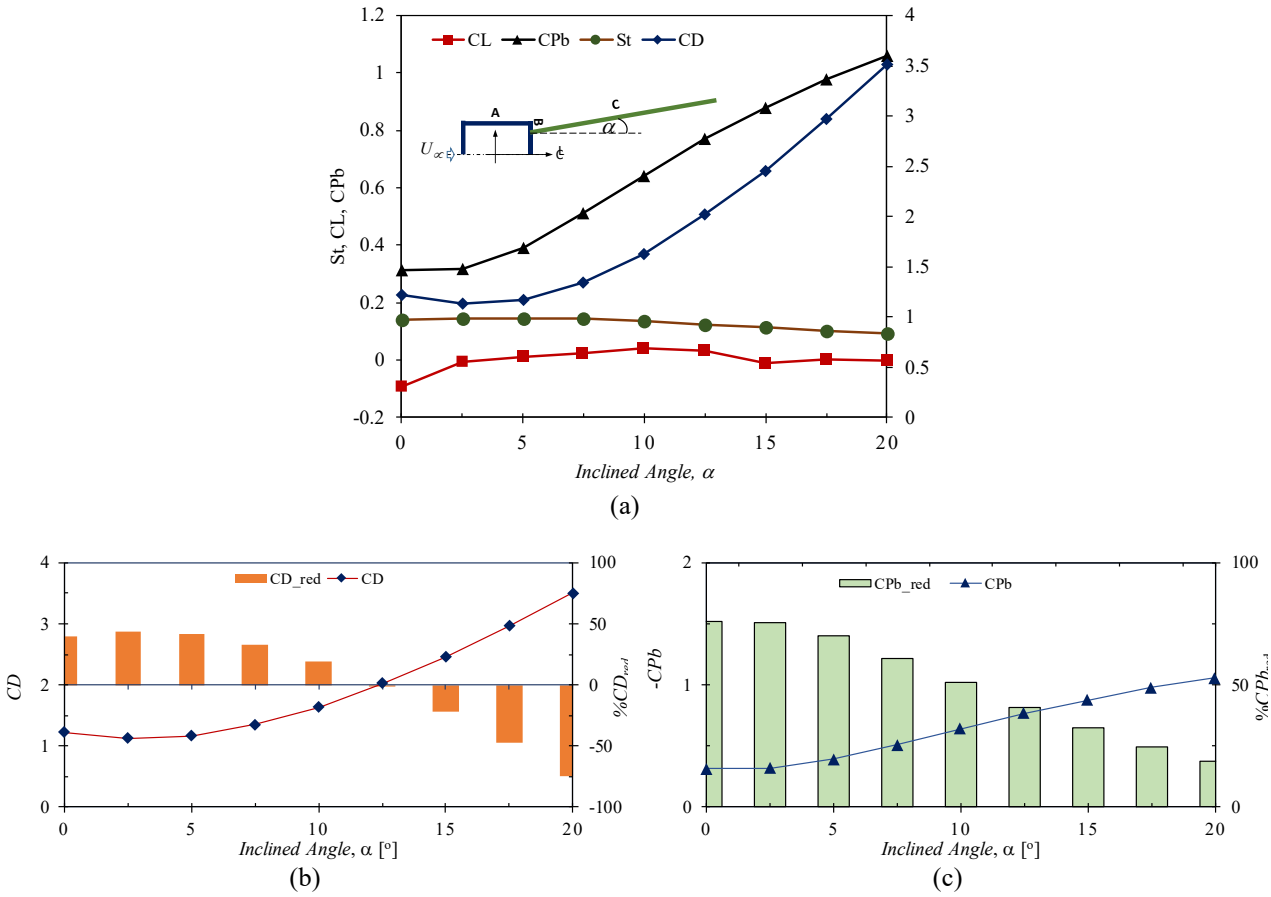

Figure 2. (a) Variation of mean flow quantities pass inclined splitter plate. (b) *CD* reduction. (c) *CP*b recovery

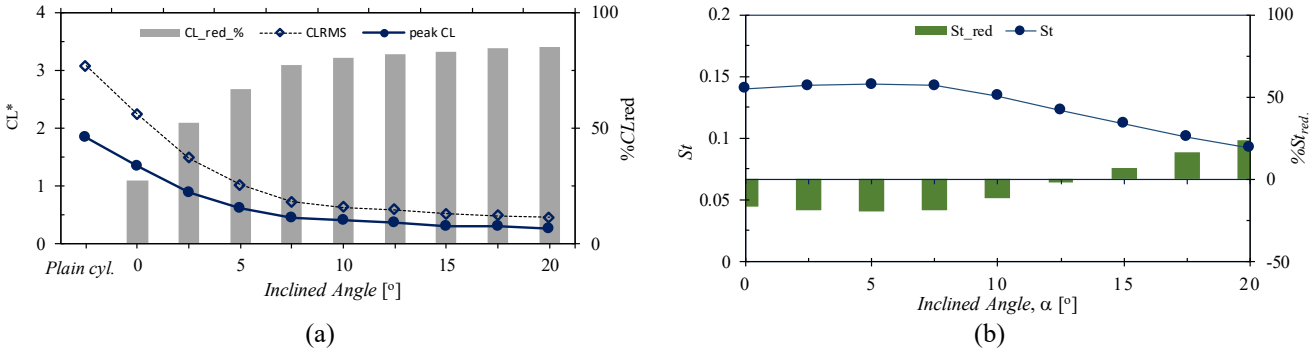

Figure 3. (a) Lift force profiles. (b) Strouhal Numbers variation

FFT power spectra analysis of lift force fluctuation was shown in Figure 4. A straight splitter plate model for a flow control showed a less sharp peak on the spectra analysis compared to the angled splitter plate. Relating to this discussion, the process meant that the straight splitter plate substantially suppressed the lift fluctuation. Inclining splitter plate created more dominant peaks, meaning a chaotic wake pattern occurred, and this process was observed that $\alpha > 10°$ showed dominant peaks with less small intrusion. Increased fluctuation in the drag force connected to higher Strouhal numbers showed more frequent vortex shedding. This unsteady drag component was added to the average drag force experienced by the object. Angled splitter plate increased *St* for $5° < \alpha < 10°$ and negated drag increment, while drag force increased consistently with inclination angle uptick ($\alpha > 10°$), even though Strouhal numbers declined. Modification of the wake by installing an inclined downstream splitter plate contributed more to the mean drag component. Moreover, the dominant peak of the *FFT* spectra of the parallel splitter plate was still identified, in comparison to a single splitter plate shown by [19] and [45].

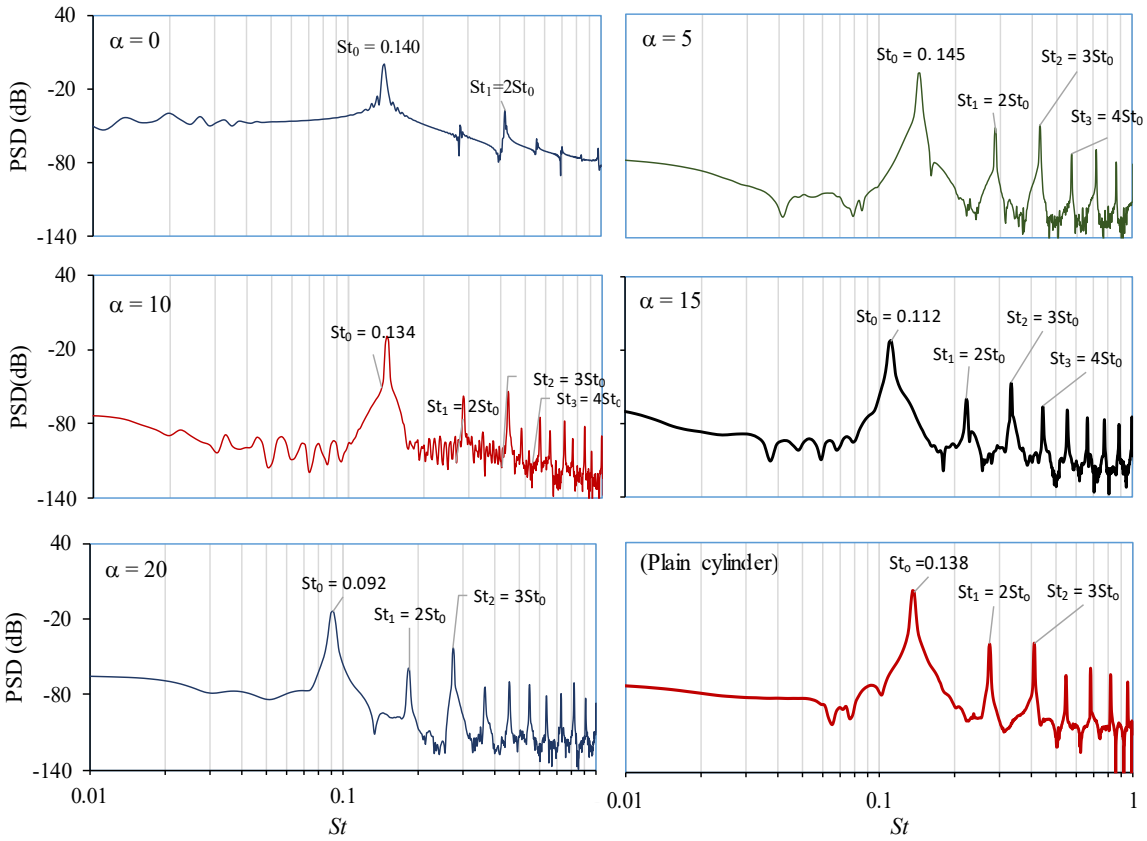

Figure 4. Power spectra density (*PSD*) of lift fluctuation for various inclined angles of splitter plate. The plain cylinder was also shown for comparison

3.2 Pressure Field

Pressure recovery due to flow separation at the cylinder's leading edge was maintained by the splitter plate through delaying detached flow, aiding recovery in the wake, and lowering the drag effect. Angled splitter plate still maintained drag reduction below the critical inclination angle and progressively nullified drag reduction out of this area. In addition, the peak of pressure recovery was relatively similar to $\alpha = 0 - 5°$, enabling the drag reduction to be sustained. Pressure distribution along the wall boundary condition of flow passing an angled splitter plate is shown in Figure 5. The inclining splitter plate recovered the pressure component of the upper wall of the boundary condition. Moreover, the separated shear layer effect at the cylinder leading edge (*A*-zone) on the gradient pressure was diminished by using a straight splitter plate, achieving drag reduction. Pressure distribution crest at the *C*-zone in Figure 5 showed pressure recovery due to the reattachment of the separated shear layer. This zone varied by distance, which depended on the splitter inclination angle.

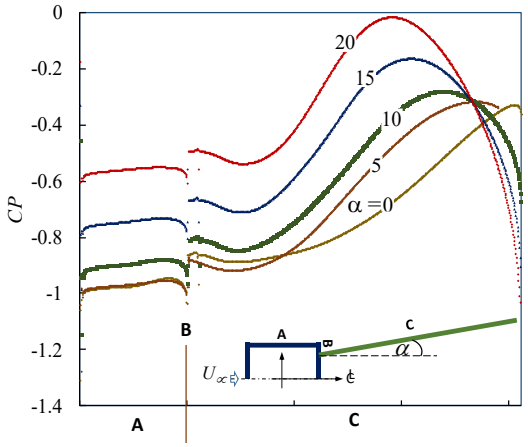

Figure 5. Time-averaged pressure distribution for various inclined angles of splitter plate

Additionally, the end valley of these lines represented the lower surface of the *C*-zone, which was closely related to negative pressure or pressure gradient increment, and this correlated to drag force increase as described previously. *B*-zone, located at the cylinder trailing edge, contributed to form the small valley of pressure distribution at *C*-zone with a similar depth pattern for all angled splitter plates with $\alpha \leq 5°$. Concerning this process, increasing the inclination angle of

the splitter plate enlarged the negative pressure at the plate's downstream, which caused the down force increment to be larger compared to a plain cylinder. Hence, the base pressure gradient for $\alpha \geq 10°$ was no longer proportional compared to the drag uptick.

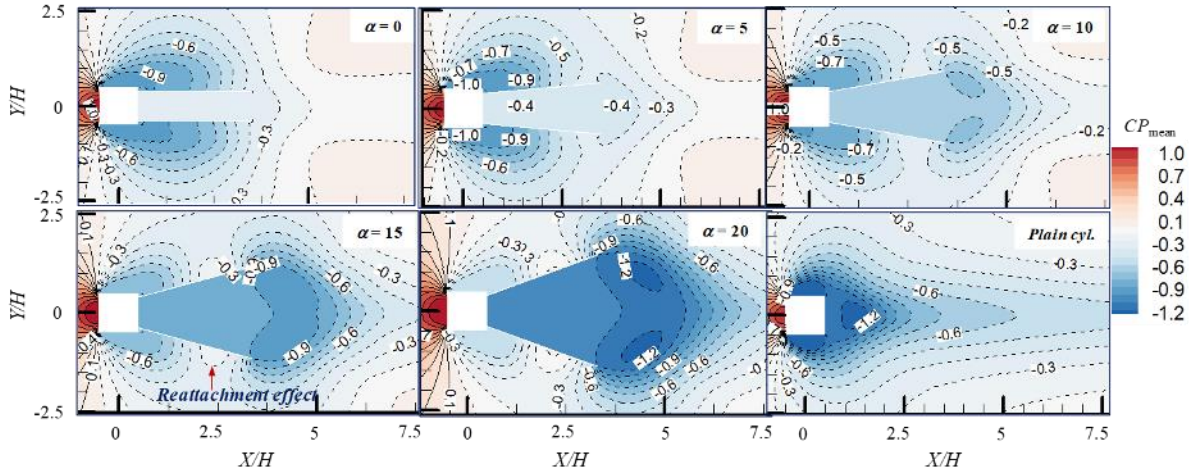

Figure 6. Time averaged flow pressure contours past inclined splitter plate

The contour profile of pressure distribution in Figure 6 represented the variation of the flow recirculation zone in Figure 9. Gradient pressure was dominated by the bubble effect at the cylinder side area for the straight splitter plate, while the plain cylinder was dominated by the pressure base. Additionally, secondary flow recirculation at the splitter trailing edge in Figure 9 was shown by a more negative pressure gradient in Figure 6. The negative pressure zone created a flow entrainment phenomenon, and the bubble zone depended on the wake size at the rear body, or cylinder side, as described previously.

3.3 Velocity Vector and the Derivatives

Variation of local velocity distributions downstream with an angled splitter plate is shown in Figure 7. Secondary separation flow at the splitter plate trailing edge created a negative zone, which led to a decrease in the mean velocity component (u). The most negative u was observed near the center of the flow recirculation region, R, as shown in Figure 9. Variation in velocity also influenced the downstream flow characteristics for plates with $\alpha > 5°$, which were considered to contribute to drag variation. In addition, the velocity behavior near the base of the cylinder remained steady at $X \leq 2.5H$, signifying that the length of the plate was effective in countering the backflow effect at the base of the cylinder. This was an essential parameter for drag reduction or Kármán vortex suppression, both of which were related to drag force magnitude [50], [51].

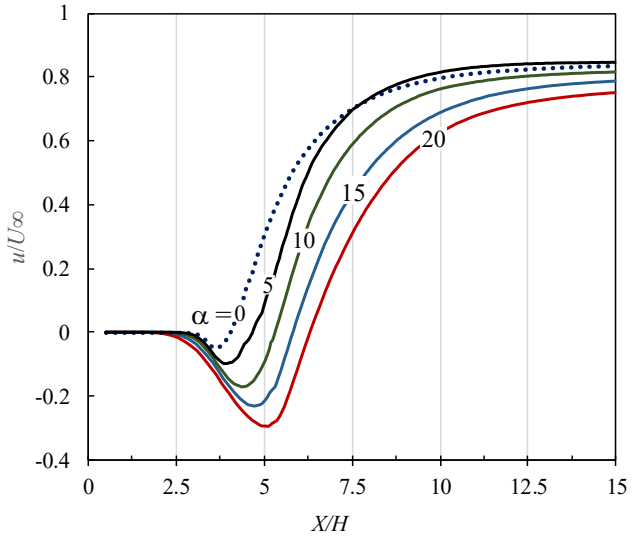

Figure 7. Streamwise local velocity variation (u/U_∞). Coordinate end of the straight splitter plate was located at *3.5*H, and slightly shifted backward by angling the splitter plate

Furthermore, the wake pattern downstream was modified by the bubble effect that created a recirculation zone. Variation of inclination angle created a varied negative pressure drop zone in the vicinity of the splitter plate end. The valleys of local velocity dropped in Figure 7, showing gradient pressure variation, meaning that as the inclination angle became higher, u near the tip of the splitter plate due to flow detached from the plate end dropped. During the process, flow recovery (u/U_∞) ranged from 70 – 80%, depending on tilting angle at $X = 15H$.

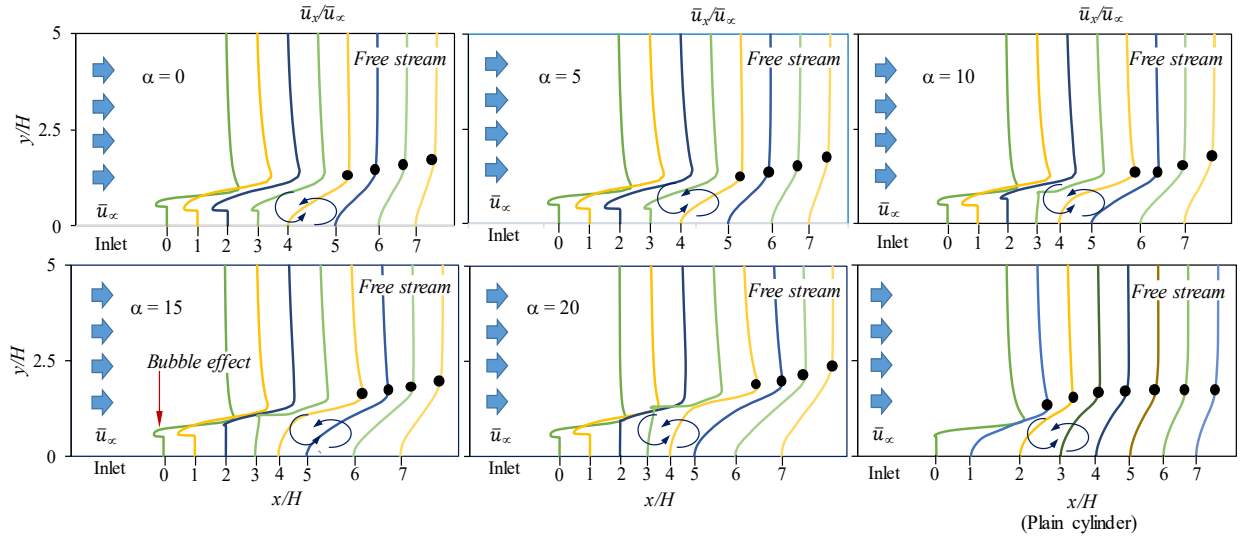

Figure 8. Time-averaged local velocity distribution past inclined splitter plate. Black dots (•) represent boundary layer formation, which was typically occurs at the splitter plate's streamwise

Figure 8 shows the velocity vector distribution at various streamwise points relating to the *y*-coordinate. The velocity profiles also provided significant insight into the variation of *u* along the coordinate, helping to understand the effects of flow separation on flow quantities such as base pressure and velocity fluctuations. Following the process, the velocity profile along the cylinder and the splitter plate ($X/H = 0$ - 3) showed different behavior from the downstream splitter plate because of the bubble's effect caused by the separated shear layer at the cylinder trailing edge. Moreover, a secondary separated sheared layer at the splitter plate tip caused fluid to accelerate, and the viscous boundary in the after plate was defined by a black dot ($x = 4H$). The negative base pressure in the viscous layer caused potent flow entrainment at the splitter base vicinity, which was characterized by reverse flow phenomena under the boundary layer zone. Additionally, variation in the inclination angle of the splitter plate affected the flow entrainment zone at the base plate, where the fluid was entrained due to a decrease in base pressure near the end of the plate.

Increasing the base pressure drop area was shown by the development of the boundary layer zone with respect to the y-coordinate, which signified an increase in downforce. The plain cylinder showed a backflow area that did not extend as far downstream compared to the cylinder with an inclined plate ($\alpha > 5°$), relative to the y-coordinate. This observation supported the drag variation discussed in the previous section, where tilting the plate at $\alpha > 12.5°$ did not contribute to downforce suppression. During the process, the recovery of the flow stream (*u*-component) past the cylinder with the splitter plate was influenced by the inclination angle of the plate. In Figure 8, fluid recirculation near the plate vicinity (approximately at $x = 3H$) differed from that of the plain cylinder, signifying potential secondary flow separation due to flow reattachment. *u* and the reversed flow near the plate, as well as further downstream, were both affected by the inclination angle.

Streamlined velocity variation past the double splitter plate was shown in Figure 9. *u* and its derivative influenced other flow features, such as pressure, and were connected to variations in drag. The cylinder with a straight splitter plate showed a symmetrical wake, signifying a stable recirculation zone after the cylinder. However, when the plate was tilted at $\alpha = 5°$, asymmetrical vorticity started to develop in the flow field, and multiple recirculation zones appeared. The wake was a flow center recirculation (R_i) that was formed in the case of flow passing through a square cylinder with an attached splitter plate. R_i was developed by the separation shear layer, which typically occurred at the cylinder's sharp corner.

Following the discussion, this study showed R_1 (primary), R_2 (secondary) recirculation was formed by the separation layer at the cylinder leading, and the splitter plate's trailing edges, respectively. R_3 was induced by trapped flow due to the presence of a double border of flow interaction. In addition, R_4 represented the effect of reverse flow recirculation that was also separated at the cylinder trailing edge. The size of R_1 was minimized, and R_2 was expanded by an angled splitter plate due to the variation of pressure recovery. R_2 size or wake width (yR) was considered to affect drag increment, which was typically induced by stronger vortex shedding and instability. The distance point of reattachment (xR) was varied with an angled splitter plate as shown in Figure 9(b), connecting to the R_1 zone size. R_2 typically occurred in long or short splitter plates ($L/H > 4$), both in single splitter and double plate, as shown in [17]. Furthermore, when a straight splitter plate was attached to the base of a square cylinder, the separated shear layers were transported and continued to roll downstream. Concerning this, the shear layers were attached to the plate, formed vortices, and interacted with the trailing edge of the splitter plate, and not with the cylinder base. The growing small-scale vortex at the cylinder base was reduced. Additionally, the secondary scale vortex was generated at the trailing edge of the plate. The process was also observed that the length size of the recirculation region (l_R) was expanded further downstream by increasing α. As the angle α increased, the wake structure became increasingly asymmetric. This observation implied that the splitter plate altered vortex formation in the cylinder wake, and was connected to the aerodynamic forces quantities. Relating to the discussion, wake size at the trailing edge was a requirement for the inclined angle increment.

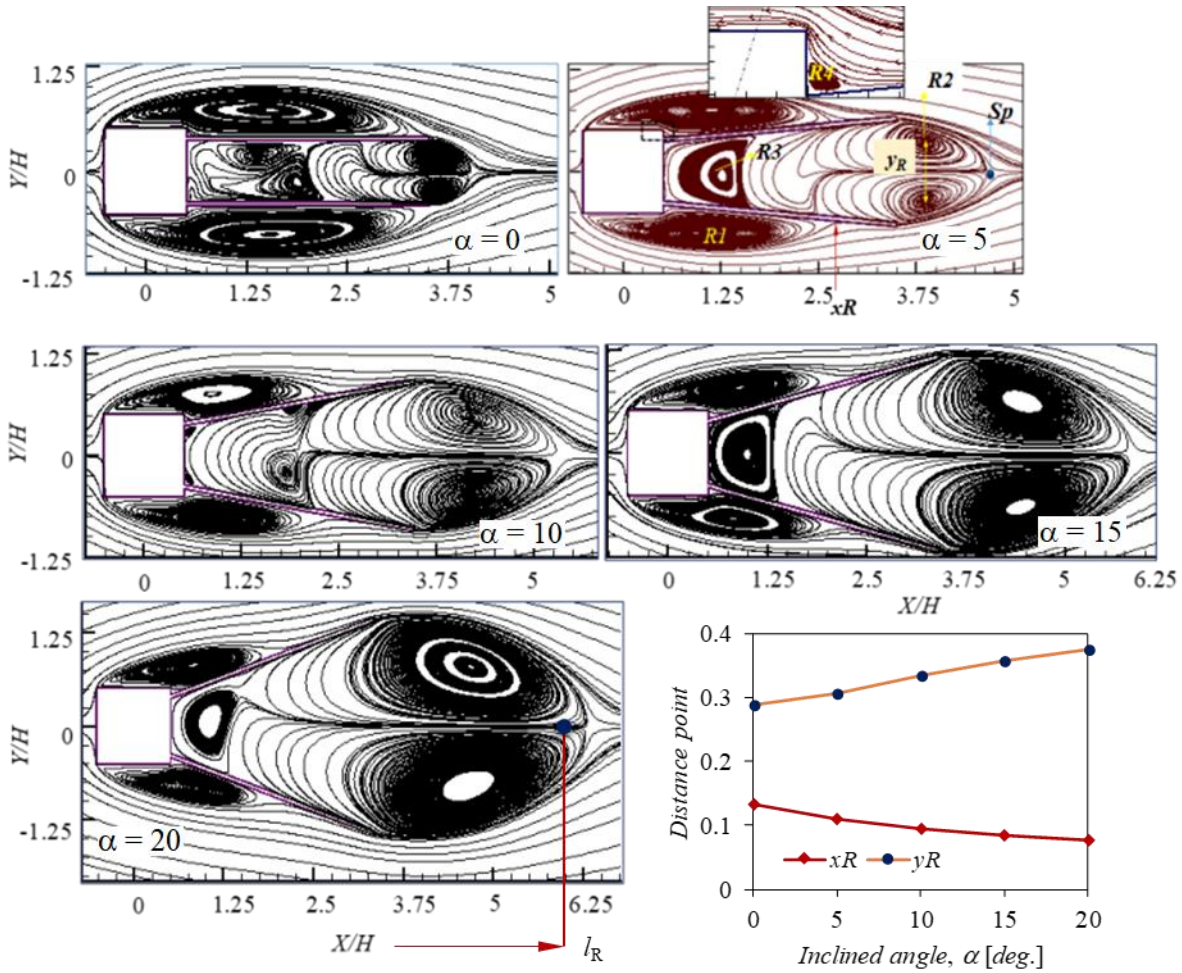

(a) (b)

Figure 9. (a) Time-averaged velocity streamline past inclined splitter plate. Close-up view in the top figure was intended to show flow behavior at the trailing edge of the cylinder center of recirculation, and saddle point, a stagnation or separation region in the wake (blue dot) is denoted by *R* and *Sp*, respectively; (b) Flow reattachment point (*xR*) and wake width (*yR*) with respect to inclined angle

3.4 Vorticity

Flow separation at the cylinder trailing edge led to swirling vortices downstream with a similar pattern as shown in Figure 10. During the analysis, Figure 10 also showed a time-averaged quantity and should be considered alongside other visualization data, including Figure 9, for a more comprehensive understanding. The pair of the swirling center was half the averaged wavelength (γ) along the simulation domain (30*H*). Once the vorticity was released at the splitter trailing edge, a Karman vortex path ramp occurred. The intensity of the initial vortex in the vicinity of the splitter plate was higher compared to consecutive shedding due to the dissipation of vortices downstream. Gradient color contours in Figure 10(a) showed vortex intensity. This dissipation effect weakened the intensity, as shown by color sharpness. The vortices were released in a pair (*P*) mode without any vortex transition. Meanwhile, Figure 10(b) showed that γ in the vortex path was typically similar for plate inclination angle of $0°<\alpha<15°$, in which deviation between distance points of γ was increased by α, and the effect of inclination angle on γ was observed for $\alpha > 10°$.

An increase in γ relating to α signified a reduction in vortex shedding frequency and an elongation of the vortex formation region. In the case of modest inclination angles ($\alpha \approx 5$–$10°$), the vortex structure was altered, as shown in Section 3.3, but still contributed to drag reduction. As α approached higher inclination angles, the vortices tended to disrupt the wake, inducing flow instability and leading to increased downforce.

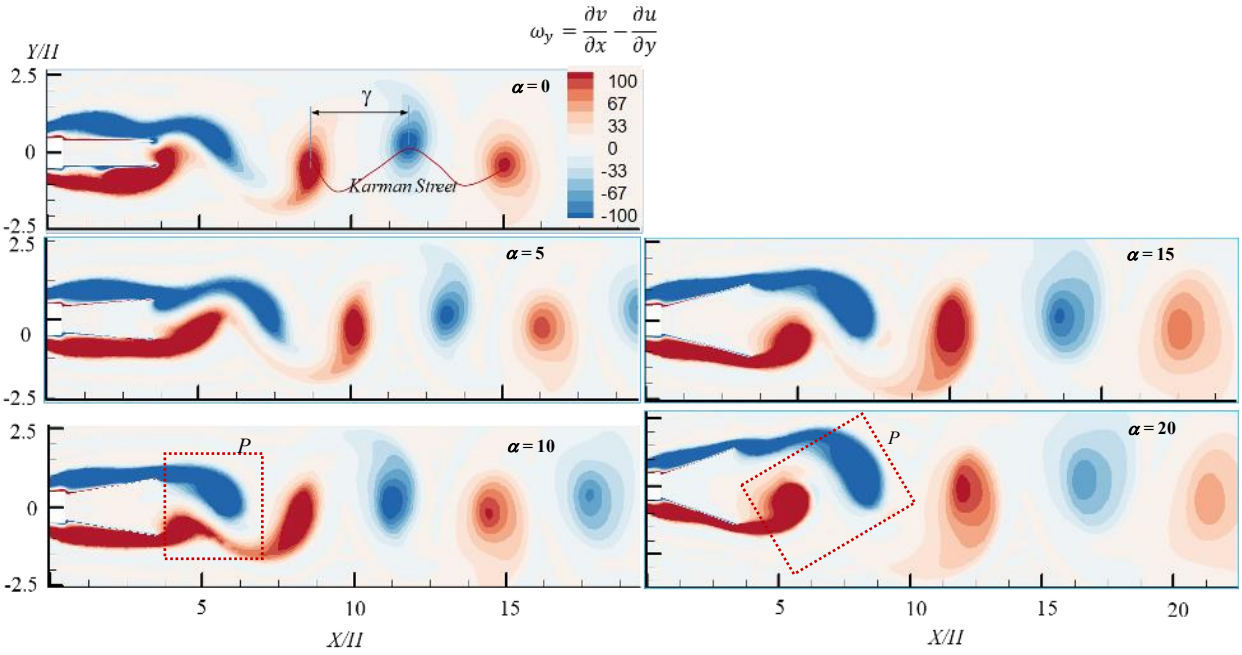

(a)

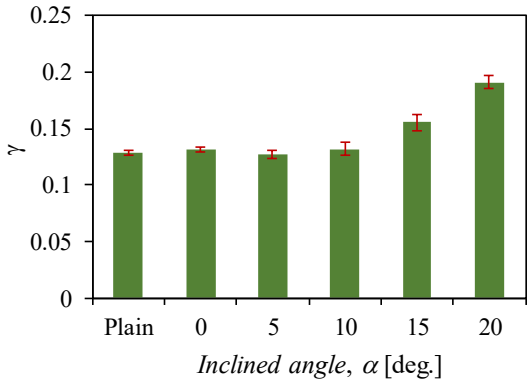

(b)

Figure 10. (a) Time averaged vorticity contours past inclined splitter plate. (b) The half wavelength averaged (γ_i) of streamwise vortices

3.5 Mean Velocity Fluctuation

The Reynolds stress component was required to describe the additional stresses in fluid flow passing through a square cylinder with an attached splitter plate due to turbulent fluctuations. These stresses occurred from the interactions between fluctuating velocity components in turbulent flow, which were decomposed by the time-averaged and fluctuating local velocity. In addition to the 2D case, there were two components of normal stress, such as u'^2 and v'^2, and shear stress of $u'v'$. The total kinetic energy for two-dimensional flow was defined by tKE = ½ ($u'^2 + v'^2$).

Figure 11 (a) showed the peak of Re stress concerning inclination angle variation of the splitter plate and was featured by total kinetic energy. Moreover, normal stress (u'^2) was more dominant at the cylinder with a straight splitter plate (α = 0°) compared to v'^2 and $u'v'$. Flow acceleration due to the separated shear layer at the cylinder leading edge led to velocity fluctuation components (u'^2, v'^2, and $u'v'$) increased in the plain cylinder and decreased by installing the splitter plate, as shown in Figure 11(b). This process implied that gradient pressure was reduced by installing a splitter plate to prevent vortex interaction in the base. Given the scenario, these components were varied by the inclination angle of the splitter plate. Crossflow fluctuation (v'^2) was consistently increased by α, while the u'^2 dropped by $\alpha < 5°$. $u'v'$ component decreased by $\alpha < 5°$ then gradually increased up to $\alpha < 20°$, with these variations closely related to changes in drag force. The peak of the Reynolds stress component typically occurred at the trailing edge of the splitter plate, where a recirculation region was formed. This study showed that the components were not solely attributed to the drag force increment for the angled splitter plate. Furthermore, the exploration also showed that tKE was lower compared to a plain cylinder, negating drag reduction at high inclination angles, such as $\alpha > 10°$.

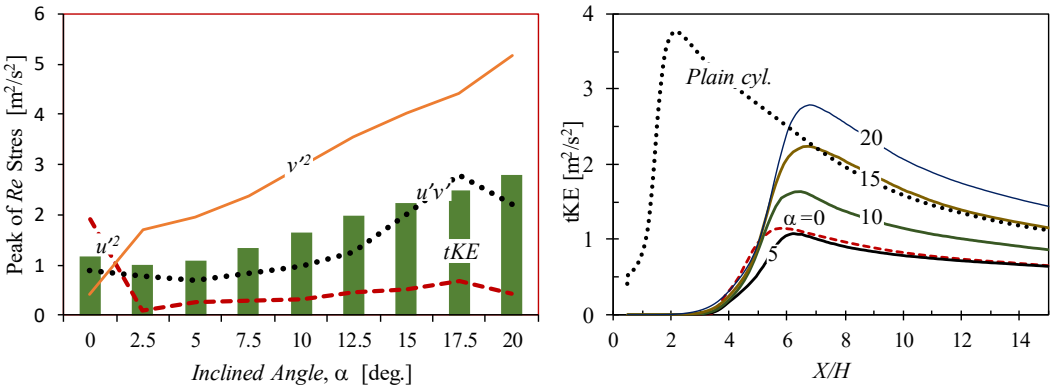

Figure 11. (a) Peak of local velocity fluctuation; (b) Total kinetic energy (*tKE)* variation along streamwise for inclined angles (α) of splitter plate

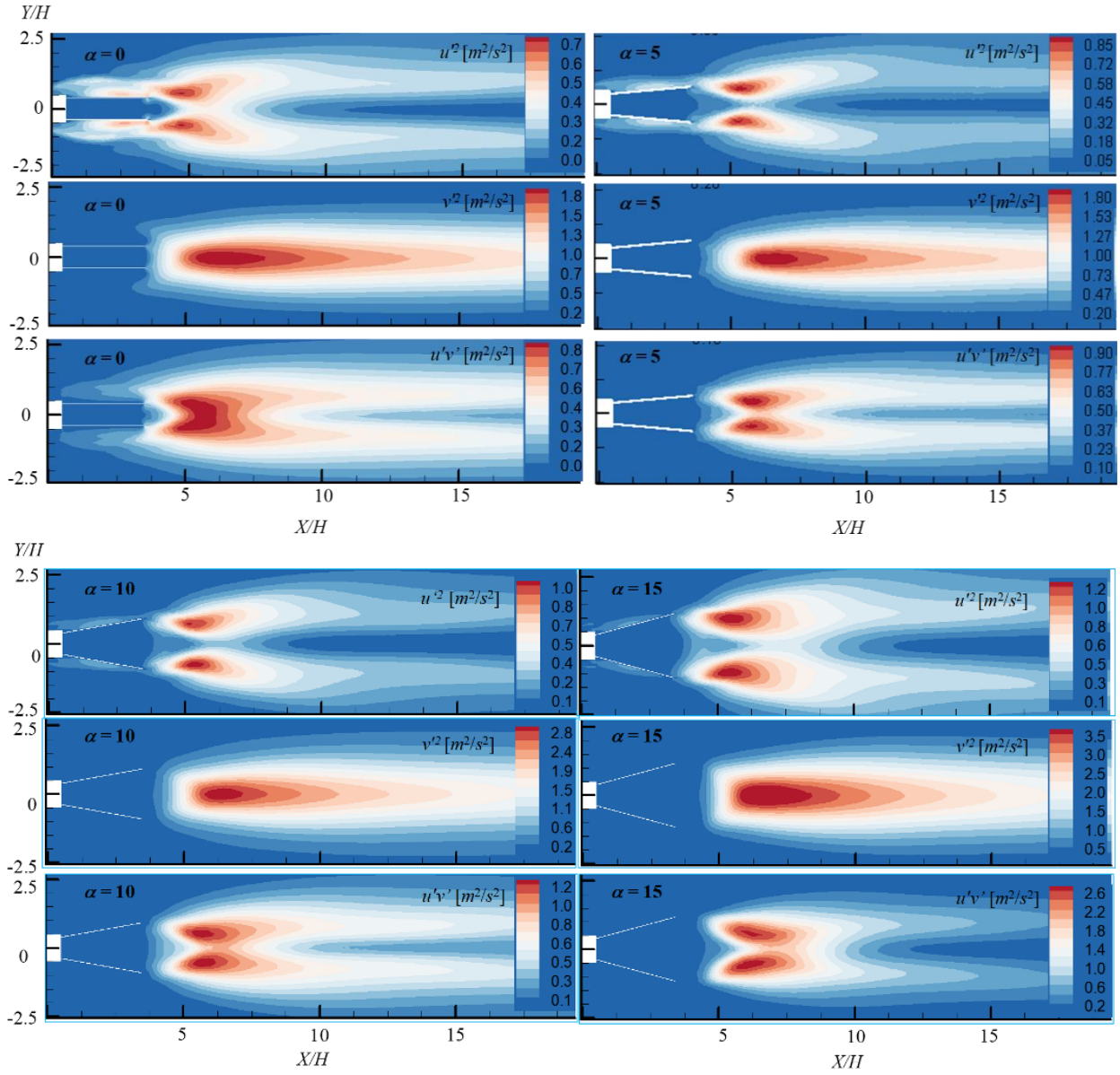

Figure 12. Contours of time-averaged Reynolds stress (normal and shear stress components) with various inclined angles

Visualization contours of Reynolds stress components were shown in Figures 12 and 13. Peak of normal stress (u'^2) was located at the splitter plate downstream at various distance points. However, cylinder leading edge separation also induced u'^2 increment, and it was minimized by α. Peak of crossflow Re stress shifted to the downstream point, and was not observed clearly at the cylinder side. Additionally, shear stress components ($u'v'^2$) for the straight plate were still

observed at the cylinder side due to primary separation (SP_1) occurring at the cylinder leading edge, where peak stress remained downstream. A single peak value of $u'v'^2$ appeared only for the straight splitter plate, and a pair of peak values appeared at the angled splitter plate. Peak distance point (l_i) of $u'v'^2$ consistently increased by $\alpha > 5°$, while u'^2 typically did not change significantly by $\alpha < 15°$, as indicated in Figure 13(a). In this study, the peak stress of v'^2 for the angled splitter plate experienced the maximum value compared to its counterparts. Peak of normal stresses was attributed to total drag, specifically for $\alpha \leq 10°$. Moreover, shear stress component ($u'v'$) was more significant for $\alpha > 10°$, showing its role in the friction coefficient (C_f), which was a component contributing to the total drag force.

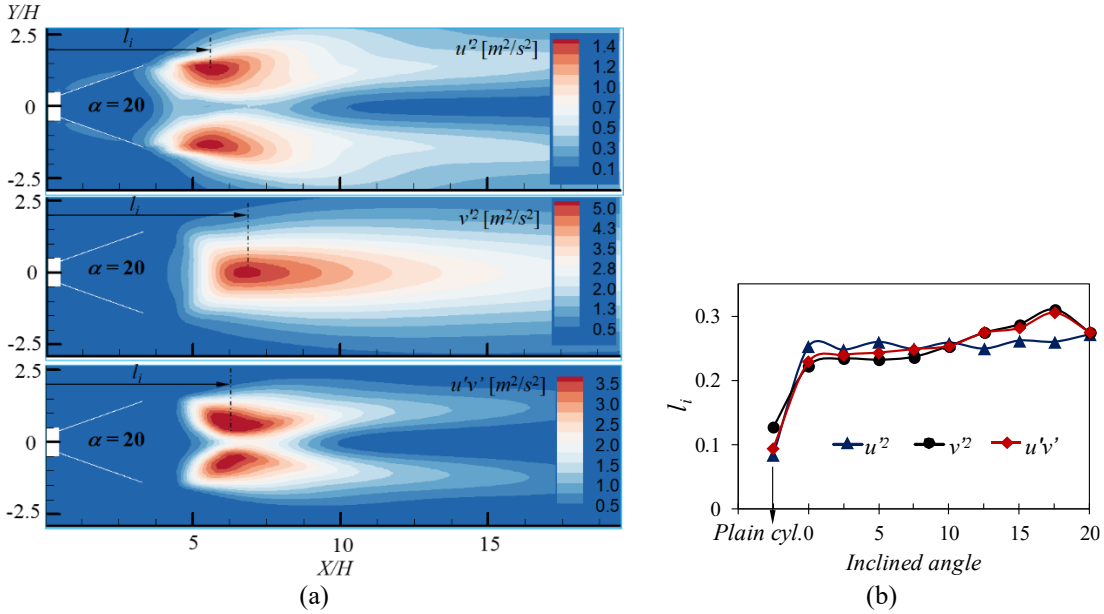

Figure 13. (a) Contours of time-averaged Reynolds stress (normal and shear stress components) with various inclined angles; (b) Time-mean of vortex center point (l_i) at streamwise

3.6 Skin Friction Coefficient

Profile of mean skin friction on a square cylinder with $\alpha = 20°$ was shown in Figure 14(a). For brevity, the figure only showed a single C_f profile due to the similarity trend for another angled splitter plate. Furthermore, the stagnation area (section A) still contributed more to C_f, and the peak of C_f was located at the primary separation point at the cylinder's sharp edge. The bubble effect due to flow acceleration at the cylinder side (section *B*) lowered the local velocity component near the wall, which led to C_f declining. A similar pattern of the C_f peak also appeared at the cylinder trailing edge with small intensity. In addition to quantifying C_f on a square cylinder with inclination angle variation of the splitter plate, Figure 14(b) shows the increment/decrement rate of C_f of the wall boundary conditions. Cylinder C_f was higher compared to the splitter plate, and decreased with inclination angle variation, showing consistent variation across all inclination angles. C_f on splitter plate uptick by increasing inclination angle, where the fluctuation was increased by α, however, the quantity was smaller compared to the cylinder.

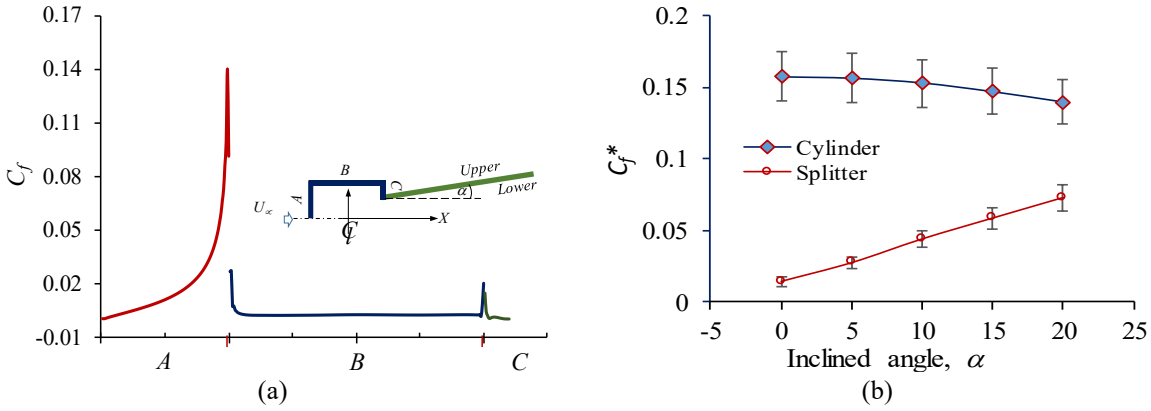

Figure 14. (a) Time-averaged skin friction (C_f) distribution along the cylinder surfaces with inclined angles α of 20°. It is noted that C_f profiles were typically similar for all inclined angles α of splitter plate except for the peak; (b) variation of C_f peak with respect to inclined angle, α

Figure 15 shows the C_f profile of the splitter plate with various inclination angles. Two major parameters that determined C_f quantity in Figure 15 included the separation point at the cylinder trailing edge and the flow reattachment

at the splitter plate (curve's valley). Moreover, the bubble size, which was caused by flow separation, determined the peak of C_f. Streamwise bubble size did not contribute to peak C_f compared to downstream bubble size. The maximum peak of C_f was found at $\alpha = 20°$, which was attributed to the size of flow recirculation at the downstream splitter plate. C_f at the base zone near the tip of the splitter plate suddenly moved to a minimum value and continuously nullified C_f near the cylinder base. Therefore, this study showed that C_f contributed less to the total CD compared to $CD_{pressure}$.

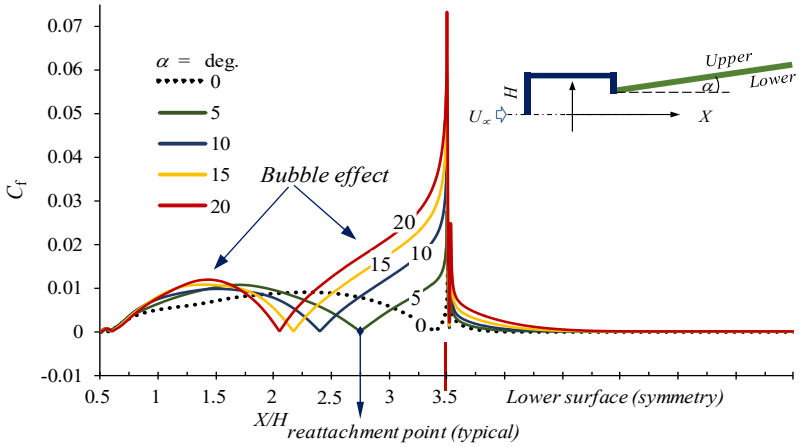

Figure 15. Time-averaged skin friction (C_f) distribution along the splitter plate for various inclined angles

4. CONCLUSIONS

In conclusion, passive control of vortex shedding behind a square cylinder with a double splitter plate at various inclination angles (α) was studied numerically for Reynolds numbers of 10^4. At different tilting angles of α, the effect of the splitter plate on the surface pressure recovery, drag and lift coefficients, and vortex-shedding phenomena were observed. During the analysis, gradient pressure recovery in the downstream of the splitter plate corresponded to a minimum drag coefficient reduction. This decrement was observed when the plate was tilted at 2.5°, resulting in a 43.8% reduction compared to the plain cylinder. Moreover, the straight splitter plate achieved a 39.4% drag reduction, nearly doubling the reduction of the single splitter plate at 20.3%. Additionally, tilting the plate by less than 5° resulted in optimum drag reduction. Suppressing lift fluctuation by tilting the plate by $\alpha \geq 10°$ did not contribute to drag reduction. For a square cylinder with a double splitter plate, the CP_b variation was not correlated with drag variation. This was conversely different from a single splitter plate, where the base pressure recovery corresponded to the variation in drag. Tilting the plates improved pressure base recovery for $\alpha \geq 5°$ with 8 – 31% in range. However, it negated the reduction of drag forces. The negation of drag reduction was considered to decrease the splitter plate base pressure, resulting in a pressure gradient increase at high splitter plate tilting angles.

Flow reattachment occurred at about $3.3H$ for (α) of the plate, and was reduced by α. This reattachment induced secondary separation at the trailing edge of the plate, generating a second vortex shedding that formed a flow-entrainment zone, and a stronger negative-pressure zone due to the bubble effect. The intensity of this phenomenon was proportional to the tilting angle of the splitter plate. Consequently, the center negative velocity component (u) shifted farther downstream by increasing α. The wake width expanded by an uptick α, while the R_1 zone decreased. Reynolds stress components verified that v'^2 was the most dominant, followed by viscous deformation ($u'v'$), and these components were attributed to drag variation. The influence of the tilting angle on the mean skin friction coefficient (Cf) was primarily related to flow separation at the edges of the cylinder and the splitter plate. Variation in C_f was generally more significant on the cylinder than on the splitter plate. However, C_f contributed only a minor share of the total drag variation, with pressure drag (CD_p) playing the dominant role.

CONFLICT OF INTEREST

The authors declare no conflicts of interest

AUTHORS CONTRIBUTION

L.O.A. Barata (Conceptualization; Methodology, Formal Analysis, Visualization, Data analysis; Writing-Original drafting)

T. Kiwata (Supervision, Software, Writing – Review editing)

Sudarsono (Supervision; Formal analysis; Supervision)

S. Alfat (Formal analysis; Visualization, Writing-Review & editing)

N. Endriatno (visualization, Writing-Review & editing)

R. Wijayanto (Software, visualization, Writing-Review & editing)

ACKNOWLEDGMENT

This work was part of the author's collaborative research with the Fluid Dynamics Laboratory, Kanazawa University, Japan. The author expresses deep gratitude to Dr. Eng. Sunichi Mizukami (Sugino Machine Ltd., Japan) and Dr. Eng. Mohamed Heragy (Assiut University, Egypt) for their valuable discussions on CFD-related topics in the past. Additionally, the authors gratefully thank Andi Yanto, one of the corresponding author's supervisees, for his assistance in building and generating the mesh construction in this study.

REFERENCES

[1] S. K. Mishra and S. Tiwari, "Wake interaction of inline circular and square section cylinder at Re = 150," in *Proceeding of 10th Thermal and Fluids Engineering Conference (TFEC)*, Connecticut: Begellhouse, 2025, pp. 625–634.

[2] S. Behara, V. Chandra, and B. Ravikanth, "Characterizing vibrations and associated wake structures of tandem square cylinders at different angles of incidence," *Physics of Fluids*, vol. 36, no. 4, pp. 1–7, 2024.

[3] F. X. Trias, A. Gorobets, and A. Oliva, "Turbulent flow around a square cylinder at Reynolds number 22,000: A DNS study," *Computers & Fluids*, vol. 123, pp. 87–98, 2015.

[4] K. Y. Billah and R. H. Scanlan, "Resonance, Tacoma Narrows bridge failure, and undergraduate physics textbooks," *American Journal of Physics*, vol. 59, no. 2, pp. 118–124, 1991.

[5] F. Duan and J. Wang, "Fluid-structure-sound interaction in noise reduction of a circular cylinder with flexible splitter plate," *Journal of Fluid Mechanics*, vol. 920, p. A6, 2021.

[6] J. Van der Krieke and G. Van Raemdonck, "Analyzing fuel savings of an aerodynamic drag reduction device with the aid of a robust linear least squares method," *SAE International Journal of Commercial Vehicles*, vol. 7, no. 2, pp. 675–684, 2014.

[7] Y. Niu and B. A. Younis, "Computational study and field implementation of methods for the control of vortex shedding from a bridge caisson," *Engineering Applications of Computational Fluid Mechanics*, vol. 19, no. 1, p. 2504677, 2025.

[8] Y. Liu, Y. Li, J. Li, J. Zhou, and X. Qiu, "The wake characteristics and hydrodynamic forces of a near-wall circular cylinder with the splitter plate," *Modern Physics Letters B*, vol. 38, no. 33, p. 2450316, 2024.

[9] W. Shan, Q. Yang, K. Guo, C. Chen, W. Zhen, and Y. C. Kim, "Across-wind response characteristics of tall-square towers in urban flow: An experimental study focused on the aeroelastic effects," *Physics of Fluids*, vol. 36, no. 3, p. 037104, 2024.

[10] W. Lei, Q. Wang, Y. Zhang, and Z. Li, "Study on VIV performance of streamlined steel box girder of a sea-crossing cable-stayed bridge," *Ocean Engineering*, vol. 295, pp. 1–8, 2024.

[11] N. Curry and P. Pillay, "Integrating solar energy into an urban small-scale anaerobic digester for improved performance," *Renewable Energy*, vol. 83, pp. 280–293, 2015.

[12] M. M. Zdravkovich, "Review and classification of various aerodynamic and hydrodynamic means for suppressing vortex shedding," *Journal of Wind Engineering and Industrial Aerodynamics*, vol. 7, no. 2, pp. 145–189, 1981.

[13] S. M. Dash, M. S. Triantafyllou, and P. V. Y. Alvarado, "A numerical study on the enhanced drag reduction and wake regime control of a square cylinder using dual splitter plates," *Computers & Fluids*, vol. 199, p. 104421, 2020.

[14] B. Barman and S. Bhattacharyya, "Control of vortex shedding and drag reduction through dual splitter plates attached to a square cylinder," *Journal of Marine Science and Application*, vol. 14, no. 2, pp. 138–145, 2015.

[15] G. R. S. Assi and P. W. Bearman, "Transverse galloping of circular cylinders fitted with solid and slotted splitter plates," *Journal of Fluids and Structures*, vol. 54, pp. 263–280, 2015.

[16] J. Y. Shao, L. Zhang, and J. D. Wen, "Vortex induced coupled vibration of an elastically mounted square cylinder with a detached solid and flexible plate," *Ocean Engineering*, vol. 283, p. 115092, 2023.

[17] G. Guan, K. He, P. Wang, H. Xu, G. Liang, Y. Wang, et al., "Study on the parameters of detached dual splitter plates and comparison with single plate for VIV suppression," *Ocean Engineering*, vol. 284, p. 115183, 2023.

[18] M. S. M. Ali, C. J. Doolan, and V. Wheatley, "Low Reynolds number flow over a square cylinder with a detached flat plate," *International Journal of Heat and Fluid Flow*, vol. 36. pp. 133–141, 2012.

[19] L. O. A. Barata, E. Ngii, T. Kiwata, and T. Kono, "Enhancing dynamic response of cantilevered rectangular prism using a splitter plate as a passive turbulence control in water tunnel," *Journal of Advanced Research in Fluid Mechanics and Thermal Sciences*, vol. 91, no. 2, pp. 1–14, 2022.

[20] L. O. A. Barata, T. Kiwata, and Sudarsono, "Micro-electricity generation from wind-induced vibration with magnetostrictive material-based energy harvester," *e-Prime-Advances in Electrical Engineering, Electronics and Energy*, vol. 9, p. 100637, 2024.

[21] T. Shima, T. Kiwata, S. Takeuchi, T. Kono, and T. Ueno, "Effect of a splitter plate on the performance of magnetostrictive flow-induced vibrational power generator using a cantilevered circular cylinder," *Transactions of the JSME (in Japanese)*, vol. 90, no. 933, pp. 23–00257, 2024.

[22] R. Natarajan, Y. Sambath, S. Chinnasamy, C. Manimuthu, A. Mohanty, and M. E. M. Soudagar, "Effect of plate length on drag reduction of square faced bluff body," in *E3S Web of Conferences*, vol. 488, p. 03012, 2024.

[23] F. Ren, F. Zhang, Y. Zhu, Z. Wang, and F. Zhao, "Enhancing heat transfer from a circular cylinder undergoing vortex induced vibration based on reinforcement learning," *Applied Thermal Engineering*, vol. 236, p. 121919, 2024.

[24] P. Dey, "Enhancement of thermo-fluid performance of square cylinder by dual splitter plates," *International Journal of Mechanical Sciences*, vol. 238, p. 107849, 2023.

[25] A. Ashouri, E. Izadpanah, Y. Amini, and S. H. Meraji, "Effects of splitter plate and mass ratio on flow-induced vibration and heat transfer characteristics of a circular cylinder in turbulent flow: A numerical study," *International Journal of Heat and Mass Transfer*, vol. 222, p. 125168, 2024.

[26] J. Y. Hwang and K. S. Yang, "Drag reduction on a circular cylinder using dual detached splitter plates," *Journal of Wind Engineering and Industrial Aerodynamics*, vol. 95, no. 7, pp. 551–564, 2007.

[27] L. O. A. Barata, T. Kiwata, A. Rachman, Samhuddin, and N. Endriatno, "Numerical investigation of flow around finite height rectangular," *CFD Letters*, vol. 15, no. 6, pp. 154–175, 2023.

[28] E. M. J. Komen, L. H. Camilo, A. Shams, B. J. Geurts, and B. Koren, "A quantification method for numerical dissipation in quasi-DNS and under-resolved DNS, and effects of numerical dissipation in quasi-DNS and under-resolved DNS of turbulent channel flows," *Journal of Computational Physics*, vol. 345, pp. 565–595, 2017.

[29] T. Kajishima and K. Taira, *Computational Fluid Dynamics*, no. 9783319762333. Cham, Switzerland: Springer International Publishing, 2017.

[30] A. Mashhadi, A. Sohankar, and M. M. Alam, "Flow over rectangular cylinder: Effects of cylinder aspect ratio and Reynolds number," *International Journal of Mechanical Sciences*, vol. 195, p. 106264, 2021.

[31] W. M. Henk Kaarle Versteeg, *An Introduction to Computational Fluid Dynamics: The Finite Volume Method*. Pearson Education Limited, 2007.

[32] Ansys.com, "36.13. Performing Time-Dependent Calculations." Accessed: Feb. 14, 2024. [Online]. Available: https://ansyshelp.ansys.com/public/account/secured?returnurl=/Views/Secured/corp/v242/en/flu_ug/flu_ug_sec_solve_calc_time.html?utm_source

[33] A. Inc., "ANSYS Fluent Theory Guide v17.1," ANSYS 17.1 Doc., vol. 15317, p. 850, 2016, [Online]. Available: http://www.ansys.com

[34] W. L. Oberkampf and T. G. Trucano, "Verification and validation in computational fluid dynamics," *Progress in Aerospace Sciences*, vol. 38, no. 3, pp. 209-272, 2002.

[35] W. L. Oberkampf and M. F. Barone, "Measures of agreement between computation and experiment: Validation metrics," *Journal of Computational Physics*, vol. 217, no. 1, pp. 5–36, 2006.

[36] H. Bai and M. M. Alam, "Dependence of square cylinder wake on Reynolds number," *Physics of Fluids*, vol. 30, no. 1, p. 015102, 2018.

[37] Okajima A, "Strouhal number of rectangular cylinders," *Journal of Fluid Mechanics*, vol. 123, pp. 379–398, 1982.

[38] S. Mizukami, "Study on the flow around the elastically supported prism and the vibration dynamics of the flow. (in Japanese)," Master Thesis, Kanazawa University, 2017.

[39] D. Yu, K. Butler, A. Kareem, J. Glimm, and J. Sun, "Simulation of the influence of aspect ratio on the aerodynamics of rectangular prisms," *Journal of Engineering Mechanics*, vol. 139, pp. 429–438, 2013.

[40] A. Sohankar, "Large eddy simulation of flow past rectangular-section cylinders: Side ratio effects," vol. 96, pp. 640–655, 2008.

[41] D. A. Lyn, S. Einav, W. Rodi, and J.-H. Park, "A laser-Doppler velocimetry study of ensemble-averaged characteristics of the turbulent near wake of a square cylinder," *Journal of Fluid Mechanics*, vol. 304, pp. 285–319, 1995.

[42] C. W. Knisely, "Strouhal numbers of rectangular cylinders: A review and new data," *Journal of Fluids and Structures*, vol. 4, pp. 371–393, 1990.

[43] K. Shimada and T. Ishihara, "Application of a modified k–ε model to the prediction of aerodynamic characteristics of rectangular cross-section cylinder," *Journal of Fluids and Structures*, vol. 16, no. 4, pp. 465–485, 2002.

[44] K. R. Sharma and S. Dutta, "Flow control over a square cylinder using attached rigid and flexible splitter plate at intermediate flow regime," *Physics of Fluids*, vol. 32, no. 1, p. 014104, 2020.

[45] A. R. Ogunremi and D. Sumner, "The effect of a splitter plate on the flow around a finite prism," *Journal of Fluids and Structures*, vol. 59, pp. 1–21, 2015.

[46] J. Wang, B. Zhou, G. Jin, Z. Liu, H. Xu, and G. Zhang, "Experimental study on the wake control of a square cylinder mounted with dual rigid/flexible splitter plates in the subcritical regime," *Ocean Engineering*, vol. 285, p. 115334, 2023.

[47] Y. Sun, J. Wang, Z. Hu, K. Lin, and D. Fan, "Transition of FIV for a circular cylinder with splitter plates," *International Journal of Mechanical Sciences*, vol. 227, p. 107429, 2022.

[48] D. Kay, M. Morris, N. Hill, G. Simbolotti, and G. Tosato, "Automotive weight and drag reduction," *The Energy Technology Systems Analysis Program*, pp. 1–7, 2011. [Online] Available: https://iea-etsap.org/E-TechDS/PDF/T18_Automotive weight and drag reduction v2bis.pdf

[49] T. Tamura and P. P. N. Dias, "Unstable aerodynamic phenomena around the resonant velocity of a rectangular cylinder with small side ratio," *Journal of Wind Engineering and Industrial Aerodynamics*, vol. 91, no. 1–2, pp. 127–138, 2003.

[50] W. S. Abbasi, S. Nadeem, A. Saleem, and H. Rahman, "Improvement of vortex shedding control and drag reduction on a square cylinder using twin plates," *The International Journal of Modern Physics C*, vol. 36, no. 4, pp. 1–2, 2025.

[51] P. Sikdar and S. M. Dash, "Effect of pitching splitter plate on the wake topology and drag reduction of two square cylinders in tandem arrangement," *Ocean Engineering*, vol. 330, p. 121283, 2025.